Aprotinin interacts with substrate-binding site of human dipeptidyl peptidase III

Agić, Dejan; Brkić, H.; Kazazić, S.; Tomić, A.; Abramović, M.

Download date / Datum preuzimanja: **2025-02-17**

Aprotinin interacts with substrate-binding site of human dipeptidyl peptidase III

Dejan Agić, Hrvoje Brkić, Saša Kazazić, Antonija Tomić & Marija Abramić

View supplementary material ⌷

Published online: 13 Jan 2019.

Submit your article to this journal ⌷

Article views: 3184

View related articles ⌷

View Crossmark data ⌷

Citing articles: 7 View citing articles ⌷

Taylor & Francis
Taylor & Francis Group

Aprotinin interacts with substrate-binding site of human dipeptidyl peptidase III

Dejan Agić[a] (iD), Hrvoje Brkić[b,c] (iD), Saša Kazazić[d] (iD), Antonija Tomić[e] (iD), and Marija Abramić[e] (iD)

[a]Department of Chemistry, Faculty of Agriculture in Osijek, Josip Juraj Strossmayer University of Osijek, Osijek, Croatia; [b]Department of Biophysics and Radiology, Faculty of Medicine, Josip Juraj Strossmayer University of Osijek, Osijek, Croatia; [c]Department of Biophysics and Radiology, Faculty of Dental Medicine and Health, Josip Juraj Strossmayer University of Osijek, Osijek, Croatia; [d]Division of Physical Chemistry, Ruđer Bošković Institute, Zagreb, Croatia; [e]Division of Organic Chemistry and Biochemistry, Ruđer Bošković Institute, Zagreb, Croatia

Communicated by Ramaswamy H. Sarma

ABSTRACT

Human dipeptidyl peptidase III (hDPP III) is a zinc-exopeptidase of the family M49 involved in final steps of intracellular protein degradation and in cytoprotective pathway Keap1-Nrf2. Biochemical and structural properties of this enzyme have been extensively investigated, but the knowledge on its contacts with other proteins is scarce. Previously, polypeptide aprotinin was shown to be a competitive inhibitor of hDPP III hydrolytic activity. In this study, aprotinin was first investigated as a potential substrate of hDPP III, but no degradation products were demonstrated by MALDI-TOF mass spectrometry. Subsequently, molecular details of the protein–protein interaction between aprotinin and hDPP III were studied by molecular modeling. Docking and long molecular dynamics (MD) simulations have shown that aprotinin interacts by its canonical binding epitope with the substrate binding cleft of hDPP III. Thereby, free N-terminus of aprotinin is distant from the active-site zinc. Enzyme-inhibitor complex is stabilized by intermolecular hydrogen bonding network, electrostatic and hydrophobic interactions which mostly involve constituent amino acid residues of the hDPP III substrate binding subsites S1, S1', S2, S2' and S3'. This is the first study that gives insight into aprotinin binding to a metallopeptidase.

1. Introduction

Dipeptidyl peptidase III (DPP III) is a metallopeptidase of the family M49 (MEROPS: https://www.ebi.ac.uk/merops/; Rawlings et al., 2018) characterized by the hexapeptide HEXXGH zinc-binding motif (Abramić, Špoljarić, & Šimaga, 2004a; Fukasawa et al., 1998). This proteolytic enzyme is considered to participate in post-proteasomal intracellular protein catabolism due to its relatively broad specificity toward peptides of different composition sized 3–10 amino acids (Abramić, Zubanović, & Vitale, 1988; Chen & Barrett, 2004). DPP III catalyzes the hydrolysis of penultimate peptide bond, liberating the dipeptides sequentially from the N-termini of its substrates. Human DPP III is the best characterized member of the family, in terms of biochemistry, structural biology and computational dynamics (Abramić et al., 1988, 2004b; Agić et al., 2017; Baršun, Jajčanin, Vukelić, Špoljarić, & Abramić, 2007; Bezerra et al., 2012; Chen & Barrett, 2004; Karačić, Špoljarić, Rožman, & Abramić, 2012; Kumar et al., 2016; Shimamori, Watanabe, & Fujimoto, 1986; Tomić, Gonzalez, & Tomić, 2012; Tomić & Tomić, 2014; Tomić, Kovačević, & Tomić, 2016). It is a monomeric acidic protein (pI~4.6) with 737 amino acids in the polypeptide chain and molecular mass of 82 500 Da (Abramić et al., 1988, 2000; Chen & Barrett, 2004). Crystal structure of ligand-free human DPP III (PDB code: 3FVY) is very

similar to the yeast enzyme (PDB code: 3CSK) showing a two-domain elongated protein molecule (Figure 1(A)) with a cleft ~40 Å wide and ~25 Å high between the lobes (Baral et al., 2008; Bezerra et al., 2012). The X-ray structure of human dipeptidyl peptidase III (hDPP III) in complex with pentapeptide ligand revealed large domain motion upon ligand binding and the formation of closed enzyme's active site (Bezerra et al., 2012). During long molecular dynamics (MD) simulations (>100 ns) of the ligand-free hDPP III, a large-scale conformational change (protein closure) has been observed (Tomić et al., 2012.) suggesting that in solution hDPP III exists in "open" and "closed" conformations.

In contrast to the cleavage potential of various peptides, human DPP III has restricted action on synthetic substrates dipeptidyl arylamides showing the preference for diarginyl arylamide (Chen & Barrett, 2004; Jajčanin-Jozić & Abramić, 2013).

We have reported previously that hDPP III can act as a post-proline cleaving enzyme on opioid tetrapeptides endomorphins, and that it cleaves endomorphin-1 at a comparable rate as serine peptidase dipeptidyl peptidase IV (DPP IV) (Baršun et al., 2007). DPP IV has pronounced specificity for dipeptide cleavage from the N-terminal of (poly)peptides when proline (or alanine) is at the penultimate position (Gabrilovac, Abramić, Užarević, Andreis, & Poljak, 2003). Until
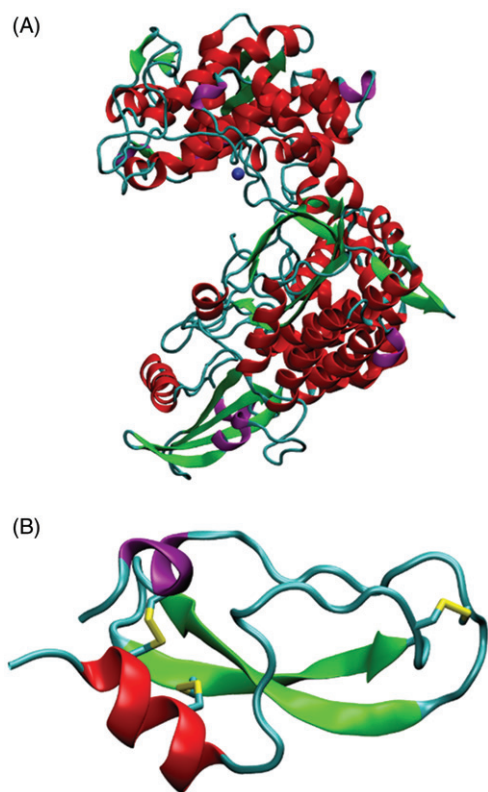
Figure 1. Schematic representation of: (A) the 3-D structure of human DPP III (PDB code 3FVY) and (B) the 3-D structure of aprotinin (PDB code 4PTI).

now, no polypeptide substrate of DPP III is known. However, competitive inhibition of hDPP III with aprotinin has been reported (Abramić, Karačić, Šemanjski, Vukelić, & Jajčanin-Jozić, 2015).

Aprotinin is monomeric, strongly basic polypeptide 58 amino acids long, derived from bovine lung tissue, also known as bovine pancreatic trypsin inhibitor (BPTI), or basic trypsin inhibitor of bovine pancreas (Ascenzi et al., 2003; Mahdy & Webster, 2004). BPTI is a natural proteinase inhibitor whose physiological function is to inhibit digestive proteinases. It is a competitive serine peptidase inhibitor of the inhibitor family I2 (MEROPS: https://www.ebi.ac.uk/merops/). Aprotinin inhibits chymotrypsin, plasmin, and kallikrein with K_i in nanomolar range, and the equilibrium constant value for the bovine trypsin-aprotinin complex is extremely low (6×10^{-14} M) (Fritz & Jochum, 1989). Aprotinin is used in selected surgical interventions because it reduces hemorrhagic complications (Ascenzi et al., 2003). Under the trade name Trasylol, aprotinin, as an antifibrinolytic molecule was used as a hemostatic drug to reduce bleeding during cardiac surgery. (Broomhead, Myers, & Mallett, 2016; Mahdy & Webster, 2004). Clinically, aprotinin is given by continuous infusion (Mahdy & Webster, 2004). It is metabolized in kidneys, where it concentrates as shown by pharmacokinetic studies (Vio et al., 1998). The investigation on cellular distribution of exogenous aprotinin in the rat kidney has shown its distribution over the cytoplasm of the proximal tubule cells where it remained intact for at least 24 h. Some aprotinin biological effects are unrelated to inhibitor function (Fritz & Jochum, 1989). Extraordinary feature of aprotinin is its

high positive net charge at physiological pH7.4 and some of its effects are or may be mediated by ionic interactions with negatively charged substances or surfaces (e.g. binding to the platelet membrane, some renal effects) (Fritz & Jochum, 1989; Vio et al., 1998).

BPTI was one of the earliest proteins whose crystal structure was solved (Deisenhofer & Steigemann, 1975; Huber, Kukla, Rühlmann, Epp, & Formanek, 1970). The 3-D structure of aprotinin contains the N-terminal 3_{10} helix, an antiparallel β sheet, an α helix placed near the C terminus, and it is stabilized by three intramolecular disulfide bonds (Figure 1(B)). Four amino acids at the N-terminus (Arg-Pro-Asp-Phe) and three amino acids at the C-terminus are extended from the compact globular structure of aprotinin. It was previously reported that a serine exopeptidase DPP IV is capable of removing the N-terminal dipeptide of aprotinin (Nausch, Mentlein, & Heymann, 1990).

Serine proteases and their protein inhibitors were extensively studied since the balance between the proteinases and their natural inhibitors is of great importance in biology. Although the inhibitors differ in size and shape, they all share the same canonical orientation of the loop binding to the proteinase (Helland, Otlewski, Sundheim, Dadlez, & Smalås, 1999). Numerous studies (crystallographic, thermodynamic, kinetic and mutational) have been performed on the protein inhibitor-serine proteinase interaction (cited in Helland et al., 1999), revealing the importance of the residue at P1 position located at center of the protein inhibitor canonical binding loop (nomenclature as described by Schechter & Berger, 1967). This residue is responsible for majority (up to 50%) of all contacts between the inhibitor and proteinase. Specificity of inhibition can be changed by a mutation at the P1 site. For instance, replacement of Lys by Val in aprotinin converts it from the trypsin inhibitor to the neutrophil elastase inhibitor. Extremely strong inhibition of various trypsins with BPTI (aprotinin; K_a in the 10^{11} to 10^{15} M^{-1} range) arises primarily from the interaction between the side chain of Lys15 at the P1 position and Asp189 at the bottom of the trypsin specificity pocket (Helland et al., 1999). Crystallographic studies of bovine trypsin-BPTI (Helland et al., 1999) and bovine chymotrypsin-BPTI complexes (Capasso, Rizzi, Menegatti, Ascenzi, & Bolognesi, 1997) showed that 13 amino acid residues of BPTI interact with the enzyme at <4 Å (Krowarsch, Zakrzewska, Smalas, & Otlewski, 2005). The residues which form the binding epitope of BPTI and interact with trypsin and chymotrypsin by non-covalent interactions are Thr11, Gly12, Pro13, Cys14, Lys15, Ala16, Arg17, Ile18, Ile19, Gly36, Gly37, Cys38 and Arg39. In both trypsin and chymotrypsin complexes with aprotinin, P1 residue (Lys15) contributes about 50% of intermolecular H-bond and van der Waals contacts, and becomes fully buried upon complex formation.

In this study, based on the known broad specificity and post-proline activity of hDPP III, we firstly investigated, by using sensitive matrix assisted laser desorption ionization-time of flight mass spectrometry (MALDI-TOF MS) methodology, whether aprotinin is in vitro substrate of hDPP III. Furthermore, we aimed to elucidate the molecular details of
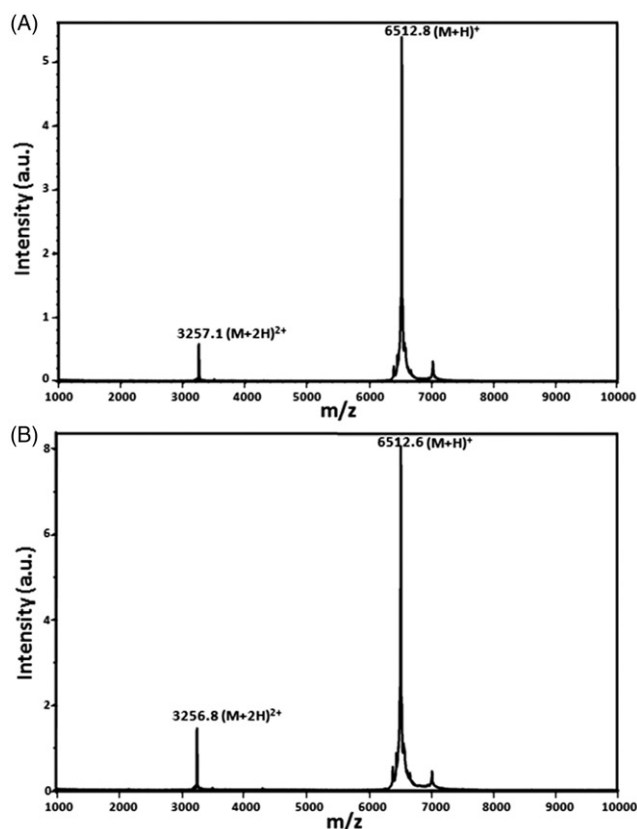
Figure 2. MALDI-TOF mass spectra of the (A) control sample of a pure aprotinin solution and (B) reaction mixture of the aprotinin and human DPP III enzyme. In both spectra, undigested aprotinin is present in two forms, as a single and doubly charged ion.

the interaction of hDPP III with this polypeptide using molecular modeling study.

2. Methods

2.1. Enzyme purification

Recombinant human DPP III was expressed and purified as described by Špoljarić et al. (2011).

2.2. Peptide hydrolysis

Aprotinin (product of Bachem) degradation by purified human DPP III was tested in reaction mixtures containing 20–300 μM aprotinin, 15 mM Tris–HCl buffer pH 7.4 (with or without 50 μM CoCl$_2$) and 1×10^{-8} M to 9×10^{-7} M hDPP III. To controls, instead of the enzyme, 15 mM Tris–HCl was added. After 18 h of incubation at 37 °C, reaction mixtures and controls were frozen. Subsequently, MALDI MS analysis was performed in sample aliquots.

2.3. MALDI-TOF MS analysis

For mass spectrometry analysis, stock solutions of the control and reaction mixture were diluted 100 times with pure water. A solution of α-cyano-4-hydroxycinnamic acid was prepared by dissolving 3 mg of the solid compound into a

50:50 solution of acetonitrile and water containing 0.1% tri-fluoroacetic acid (TFA). During sample preparation, 1 μL of the diluted solution was deposited onto MALDI target plate, each sample at the separate spot, and a 1.0 μL aliquot of MALDI matrix solution was added and the resulting droplet was left to crystallize by air drying. Mass spectra were acquired on a Microflex LT (Bruker Daltonik, Bremen, Germany) MALDI-TOF mass spectrometer operated in positive linear mode.

2.4. System preparation for molecular modeling study

The crystallographically determined structures of ligand-free human DPP III in its "open" form (PDB code 3FVY, resolution 1.9 Å) and bovine aprotinin (PDB code 4PTI, resolution 1.5 Å) were obtained from the Protein Data Bank (https://www.rcsb.org) and used as starting structures. Prior to docking and MD simulations, amino acid residues missing in 3FVY, Pro224-Asp227, were modeled using the program Modeller9v2 (Webb & Sali, 2016). The crystallized water molecules present in both structures as well as chloride and magnesium ions in 3FVY were removed. All Glu and Asp residues are negatively charged (−1) and all Arg and Lys residues are positively charged (+1), as expected at physiological conditions.

2.5. Docking

The AutoDock (AutoDock Vina version 1.1.2 plugin in the PyMol, Schrödinger, LLC, New York, NY, 2015) (Trott & Olson, 2009) software was used to search the best pose of aprotinin inside the binding site of enzyme structure. The docking box was chosen to be in the center of the gap between the two enzyme subunits, and the size of the box was $100 \times 100 \times 100$ Å^3. The best model according to the lowest interaction energy among the aprotinin and the residues inside the active site of hDPP III was used as an initial point for MD simulations.

2.6. MD simulations

Prepared hDPP III-aprotinin complex, as well as the ligand-free hDPP III was parametrized using the ff14SB force field (Maier et al., 2015) while for the zinc cation, Zn^{2+} parameters derived in previous work were used (Tomić et al., 2012.). Only the nonbonding parameters were used for Zn^{2+} ion, namely: charge 2.0e, VdW radius 1.22 Å and VdW energy well 0.250 kcal/mol. Histidines protonation site was determined according to their ability to form hydrogen bonds (H-bonds) with neighboring amino acid residues. The systems were then solvated with a truncated octahedron box of TIP3P (Jorgensen, Chandrasekhar, Madura, Impey, & Klein, 1983) water type molecules. Besides water molecules, Na$^+$ ions were added to neutralize the systems and placed in the vicinity of charged amino acids at the protein surface. Periodic boundary conditions were used and the electrostatic interactions were calculated using the particle-mesh Ewald method (Darden, York, & Pedersen, 1993). The real part
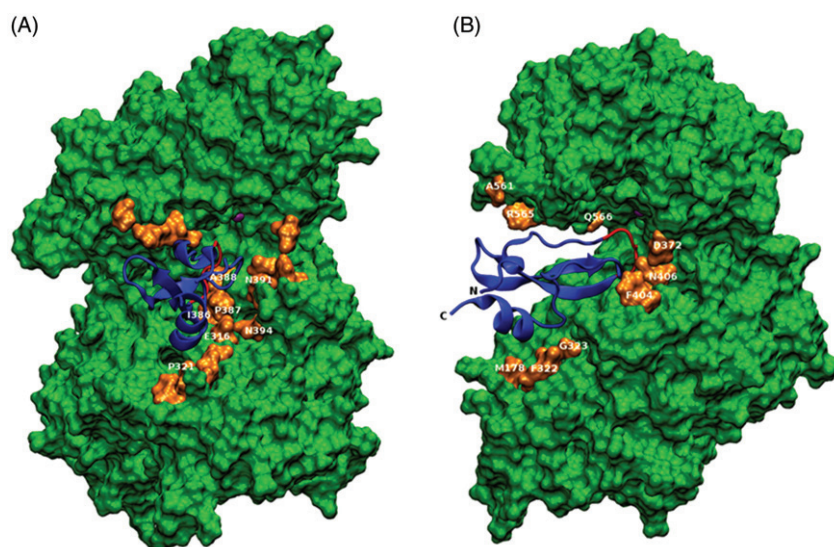
Figure 3. Binding pose of aprotinin into the topographical surface of hDPP III obtained by molecular docking. (A) and (B), the overall structure of the hDPP III-aprotinin complex in two different views.
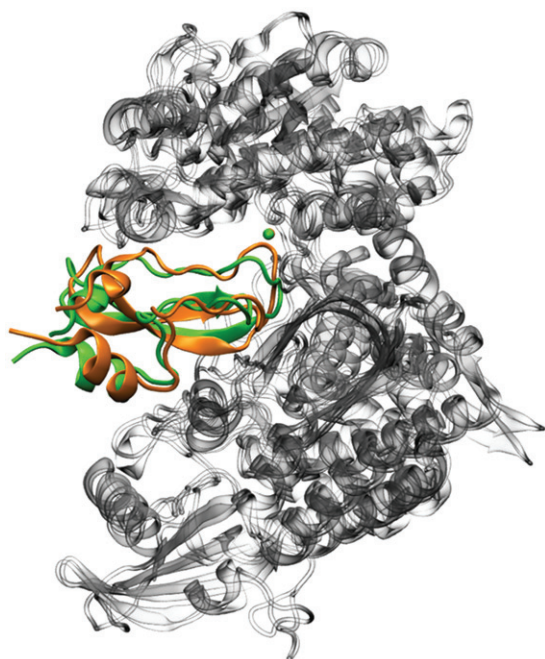

Figure 4. Overlay of the backbone atoms of the hDPP III in the complex with aprotinin obtained by molecular docking and after 200 ns of MD simulations .

contributions to electrostatic and van der Waals interactions were calculated within a cutoff radius of 11 Å. The solvated systems were then minimized in three cycles with different constraints. In the first cycle (1500 steps), water molecules were relaxed, while protein and zinc atom were constrained using a harmonic potential with a force constant of 32 kcal/(mol Å^2). In the second (2500 steps), and the third cycles (1500 steps), the same constant was applied to the zinc atom while only the protein backbone was constrained with 32 and 10 kcal/(mol Å^2), respectively. The energy minimization procedure, consisting of 470 steps of steepest descent followed by the conjugate gradient algorithm for the remaining optimization steps, was the same in all three cycles. The minimized system was firstly heated from 0 to 300 K during 30 ps using *NVT* conditions and then equilibrated 300 ps during which the initial constraints on the protein and the metal ion were used. Finally, water density adjustment and productive MD simulations were performed at constant temperature and pressure (300 K and 1 atm) using *NPT* conditions without any constraints.

The temperature was held constant using Langevin dynamics with a collision frequency of 1 ps^{-1}. Bonds involving hydrogen atoms were constrained using the SHAKE algorithm (Ryckaert, Ciccotti, & Berendsen, 1977). Simulations of complex and ligand-free hDPP III were performed within the program package AMBER14 (http://ambermd.org) (Case et al., 2014). Trajectories were 200 ns long, with a time step of 1 fs, and structures were sampled every 1 ps.

3. Results and discussion

3.1. Aprotinin interacts with, but is not degraded by human DPP III

We have recently shown that aprotinin acts as a competitive inhibitor of hDPP III hydrolytic activity, with a K_i value of 11.7 µM at physiological pH 7.4 (Abramić et al., 2015). To check whether this polypeptide could be cleaved by this enzyme, we performed long incubations with a high concentration of hDPP III, followed by MALDI-MS analysis of reaction mixture aliquots, as described in *Methods*. However, no enzymatic degradation of aprotinin was observed. As shown in Figure 2 illustrating one experiment, identical MS spectra were obtained for the reaction mixture and control sample without the enzyme. A major peak was observed at 6513 Da, and, at 3257 Da, single peak of a doubly-charged ion. No peak corresponding to the expected product of DPP III catalyzed hydrolysis of aprotinin, N-terminal Arg-Pro dipeptide (272 Da, the range not shown in the figure) was observed.
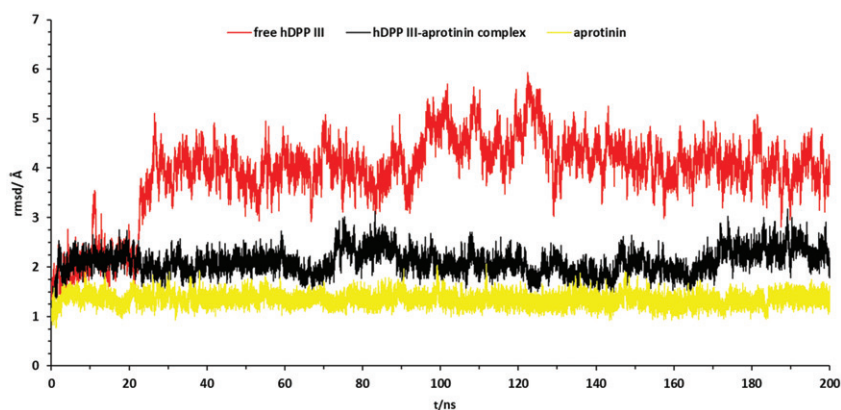
Figure 5. Rmsd profiles of the DPP III and aprotinin backbone obtained from MD simulations of ligand-free hDPP III and hDPP III-aprotinin complex.
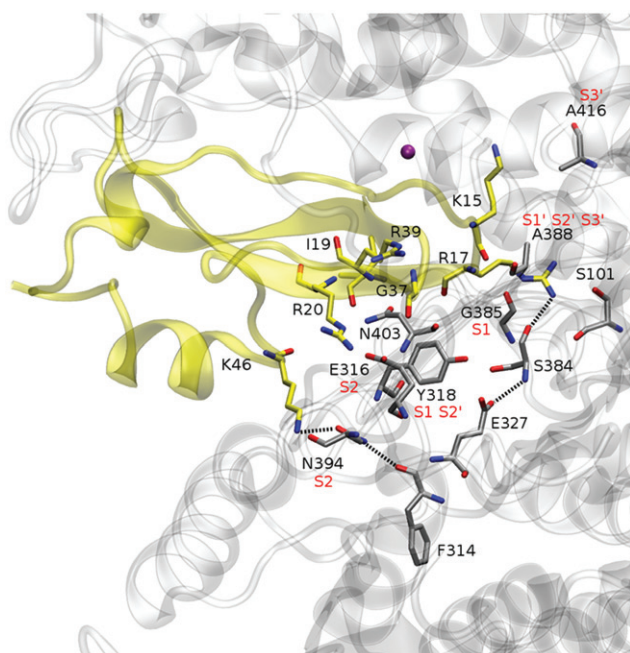

Figure 6. Amino acid residues of aprotinin that form hydrogen bonds with amino acid residues from enzyme binding site are shown in the complex structure obtained after 155 ns of MD simulations. The H-bond network K46-N394-F314 and R17-S384-E327, shown as black dashed lines, stabilizes aprotinin in the enzyme binding site. The zinc cation is shown as a sphere. Substrate binding subsites S2, S1, S1', S2' and S3' are indicated. The hydrogen atoms are not shown for clarity.

3.2. Molecular modeling of human DPP III-aprotinin interaction

To further investigate interaction of hDPP III with aprotinin, we combined docking with MD simulations. Since the aprotinin molecule has a length of 29 Å, and a diameter of 19 Å (Fritz & Jochum, 1989), we have used "open" (ligand-free) form of hDPP III for docking. In contrast to the mode of interaction with serine endopeptidases, aprotinin has been shown to interact with the active center of DPP IV by its free N-terminus (Arg1-Pro2 residues) (Engel et al., 2006). Since DPP III and DPP IV are exopeptidases acting on free amino-end of their peptide substrates, we expected similar interaction mode of aprotinin with hDPP III. However, the best binding pose obtained by molecular docking revealed that hDPP III does not bind aprotinin's amino-end. As shown in

Table 1. Populations of the selected intermolecular hydrogen bonds (HB) and hydrophobic interactions (HI) averaged over 200 ns long MD simulations of the hDPP III-aprotinin complex.

Aprotinin residue		hDPP III residue		HB (%)	HI (%)
Asp3	Side	Ser497	Side	7.5	–
Glu7	Side	Ser500	Side	–	28.5
Pro8	Side	Thr501	Side	–	12.2
Pro8	Main	Ser504(S2)	Side	1.2	–
Tyr10	Side	Ser504(S2)	Side	–	74.9
Tyr10	Side	Ala567	Side	–	60.9
Gly12	Main	His568 (S1', S2')	Side	2.6	6.7
Pro13	Side	Leu413	Side	–	4.4
Pro13	Side	Glu508 (S2, S1)	Side	–	1.0
Cys14	Side	Ala388(S1',S2', S3')	Side	–	35.1
Lys15	Main	Ala388(S1',S2', S3')	Main	88.3	–
Lys15	Main	Ala416(S3')	Main	5.2	–
Ala16	Side	Gly385	Main	–	32.1
Arg17	Side	Ser101	Main	59.3	–
Arg17	Main	Ser108	Side	5.7	–
Arg17	Side	Phe109(S2')	Side	–	41.5
Arg17	Side	Ser384	Main	74.6	–
Arg17	Main	Gly385	Main	75.2	–
Arg17	Side	Ile386(S3')	Side	–	90.7
Ile18	Side	Glu316(S2)	Side	–	88.8
Ile18	Side	Tyr318(S1, S2')	Side	–	43.4
Ile18	Side	Gly385	Main	1.0	64.3
Ile18	Side	Pro387(S1, S1', S2')	Side	–	21.5
Ile19	Side	Phe109(S2')	Side	–	18.6
Ile19	Main	Tyr318(S1, S2')	Side	2.5	–
Arg20	Side	Glu316(S2)	Side	47.8	–
Lys26	Side	Asn563	Side	1.0	1.7
Gly36	Main	Pro387(S1, S1', S2')	Side	0.9	1.8
Gly36	Main	Ala388(S1',S2', S3')	Side	3.0	–
Gly37	Main	Asn391(S2)	Main	8.6	–
Gly37	Main	Asn391(S2)	Side	7.6	–
Gly37	Main	Asn406	Side	1.1	–
Cys38	Side	Asn406	Side	–	51.4
Arg39	Side	Asp372	Main	1.7	–
Arg39	Main	Asn406	Side	42.1	–
Arg42	Side	Asp496(S2)	Main	1.3	–
Lys46	Side	Asn394(S2)	Main	44.7	–
Ser47	Side	Phe322	Main	11.8	–
Ser47	Side	Phe322	Side	–	5.8

HB were calculated with CPPTRAJ using default parameters. HB and HI with distances below 2.5 and 3.5 Å, respectively, are listed in the table. Corresponding hDPP III substrate binding subsites are given in brackets.

Figure 3(A,B), amino acid residues lining the hDPP III inter-domain cleft make numerous H-bonds and hydrophobic interactions with the aprotinin including canonical binding loop (residues [13]PCKAR[17]). At the same time, N-terminus of aprotinin is far away (31.7 Å) from the hDPP III active-site zinc, and together with the C-terminus extends from the substrate binding cleft (Figure 3(B)). This is in agreement
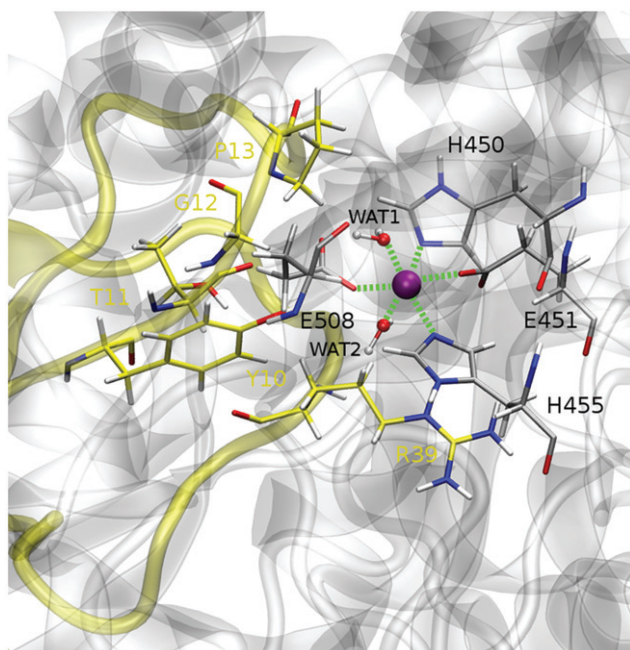
Figure 7. The zinc coordination and the close aprotinin residues in the structure obtained after 200 ns of MD simulations of the hDPP III complex with aprotinin. The zinc cation is presented as a sphere, while dashed lines represent zinc coordination with electron donors.

with our experimental finding that aprotinin is not cleaved with hDPP III.

In order to refine the docking result, we performed 200 ns long MD simulations. As can be seen from Figure 4, by docking predicted binding pose is similar to that found in the structure obtained after 200 ns of MD simulations. Moreover, in the binding pose obtained after MD simulations aprotinin interacts with more amino acids residues from the "upper" and "lower" protein domain than in the binding pose obtained by docking.

3.3. Influence of aprotinin binding on hDPP III protein structure and zinc coordination

According to the comparison of the root mean square deviation (rmsd) profiles determined by MD simulations of the ligand-free and complexed enzyme, aprotinin binding to hDPP III has a significant effect on protein stabilization (Figure 5). Namely binding of aprotinin molecule deep into the inter-domain cleft (Figure 3) accompanied by its interactions with the enzyme active site and the amino acid residues from "upper" and "lower" protein domains (Figure 6), hinder the inter-domain motion and stabilized hDPP III in an open form (Figure S1 in the supplement).

In line with this is significantly smaller globularity of the aprotinin complex with hDPP III than of the ligand free-protein (Rg obtained after 200 ns of MD simulations of complexed protein is about 28.4 Å, while for the ligand-free protein is about 27.5 Å) (Figure S2 in the supplement). Further on, binding of aprotinin had no influence on the protein secondary structure (Table S1 in the supplement) neither on the 3 D structure of "upper" and "lower" domain (not shown).

During the whole period of MD simulation of hDPP III-aprotinin complex the zinc cation was mostly six-coordinated by two glutamates (Glu451 and Glu508), two histidines (His450 and His455) and two water molecules (Figure 7). The zinc cation is coordinated with ε nitrogen atoms of H450 and H455 during entire MD simulation (left chart of Figure S3A in the supplement). Initial bidendate coordination (first 60 ns of simulations) of the zinc cation by Glu451 and Glu508 changed during the simulation to monodentate, with OE1 and OE2 atoms exchanging in the metal coordination (left chart of Figures S3B and C in the supplement). Six-coordinated zinc cation has also been observed during MD simulations of hDPP III in complex with inhibitor (benzimidazole derivative) (Rastija et al., 2015) and the ligand-free hDPP III (Tomić et al., 2012). Although the residues Tyr10 to Pro13, and Arg39 of aprotinin are in the vicinity of the catalytic zinc ion (minimal distance of ∼4.7 Å, measured between the zinc cation and hydroxyl group of Tyr10) (Figure 7), results of MD simulations imply that the binding of aprotinin into the enzyme active site has no significant effect on the zinc ion coordination compared to the zinc ion coordination of ligand-free hDPP III (for comparison see left and right charts of Figures S3 A–C in the supplement). This is also confirmed by the rmsd analyses of Zn^{2+} and its coordination sphere for both ligand-free and complex that is given in Figure 8.

3.4. Analysis of protein–protein interactions

Analysis of protein–protein interactions during MD simulations has revealed that hDPP III-aprotinin complex is mainly stabilized by H-bonds and hydrophobic interactions.

Hydrogen bonding mostly engaged Lys15 and Arg17 from the aprotinin binding epitope (important for inhibitory function with serine endopeptidases) with amino acid residues that are constituents of human DPP III S1, S1', S2, S2' and S3' substrate binding subsites (Bezerra et al., 2012; Kumar et al., 2016), and with Ser101 and Ser384 (Table 1 and Figure 6). In addition, hydrogen bonding between Arg39 from aprotinin and Asn406 which is not part of any of the hDPP III substrate binding subsites, significantly contributed to ligand stabilization. Aprotinin (mainly by Ile19, Arg20, Gly37 and Lys46) participates in hydrogen bonding with residues from the enzyme S1 and S2 subsites, part of which is Tyr318, a functionally important and evolutionary conserved residue in M49 family (Salopek-Sondi et al., 2008; Tomić et al., 2011). It is important to notice that free N-terminus of aprotinin is not bound in the enzyme S2 subsite, like it is the case with a true hDPP III substrates (Kumar et al., 2016), which explains the lack of enzymatic cleavage.

Furthermore, formation of the Arg17-Ser384 and Lys46-Asn394, aprotinin-enzyme, H-bonds is accompanied by formation of the intramolecular Ser384-Glu327 and Asn394-Phe314 H-bonds (Figure 6 and left chart of Figure S4A and B in the supplement). Formation of these bonds is also confirmed by radial distribution function (RDF) analyses shown on the right chart of Figure S4A and B, that has very well defined maximums below 2 Å. These interactions probably
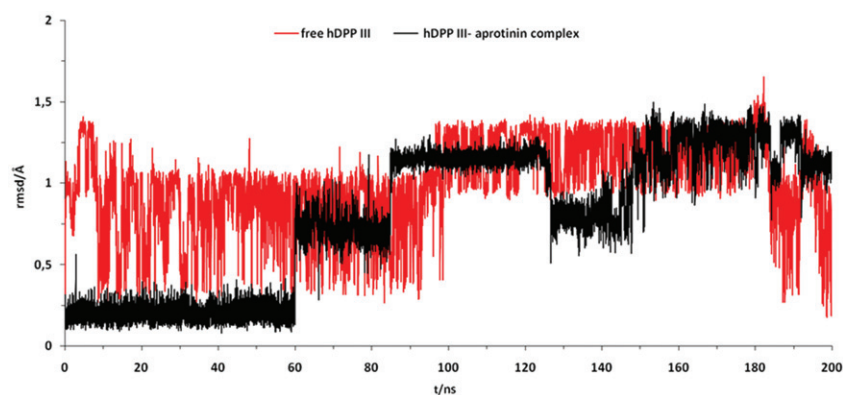
Figure 8. Rmsd profiles of the Zn^{2+} and its coordination sphere obtained from MD simulations of ligand-free hDPP III and hDPP III-aprotinin complex.
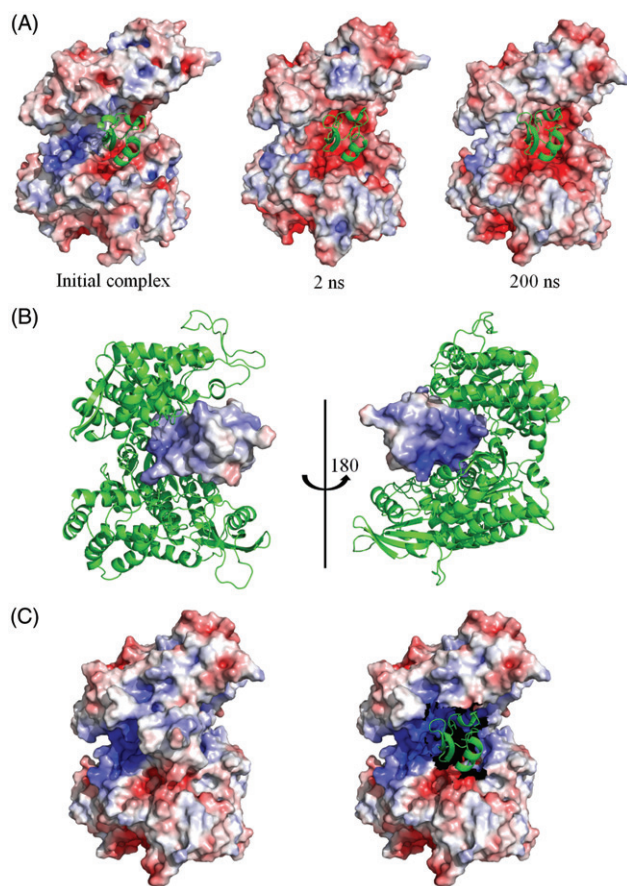

Figure 9. Electrostatic potential surfaces, calculated by the APBS module as implemented in PyMol: A) of the enzyme molecule extracted from the initial complex structure and the structures obtained after 2 and 200 ns of MD simulations (aprotinin is shown in cartoon representation), B) of the aprotinin molecule extracted from the structure of the complex obtained after 200 ns of MD simulation (hDPP III is shown in cartoon representation, two different views are given), and C) of the hDPP III-aprotinin complex, structure obtained after 200 ns of MD simulations (on the right image aprotinin is shown in cartoon representation to enable better view of the electrostatic potential surface of the enzyme molecule). The ion concentration, positive (radius 2.0 Å) and negative (radius 1.8 Å), was 0.05 M, and the protein and solvent (radius 1.4 Å) dielectric constants were set to 2 and 78, respectively. Figures are made by program PyMol.

Figure 10. Positively charged amino acids of aprotinin Arg39, Lys41 and Lys46 form electrostatic interactions (dashed lines) with hDPP III residues Asp372, Asp496 and Asp396, respectively. Optimized structure obtained after 140 ns of MD simulations was used as a reference structure for displaying electrostatic interactions.

Table 2. Solvent accessible surface area (*SASA*) determined by the programs Naccess version 2.1.1.1 using a probe with the same radius as water (1.4 Å).

	$\Delta SASA(\text{complex}_{200ns}-\text{complex}_{start})$			$\Delta SASA(\text{complex}_{2ns}-\text{complex}_{start})$		
Contribution	All	Enzyme	Aprotinin	All	Enzyme	Aprotinin
All-atoms	−1020.11	−927.4	−92.71	−1352.31	−1415.62	63.31
Side-chain	−850.22	−793.75	−56.47	−1187.19	−1313.92	126.73
Main-chain	−170	−133.79	−36.21	−164.97	−101.62	−63.35
Non-polar	−96.36	−153.72	57.36	−241.99	−411.69	169.7
Polar	−923.89	−773.85	−150.04	−1110.49	−1004.12	−106.37

Differences with regard to the initial complex structure (starting complex structure used for molecular modeling study) are shown. Beside $\Delta SASA$ values for the complex (ALL), we also show $\Delta SASA$ values obtained only for enzyme or aprotinin residues.

have an effect on aprotinin stabilization in the enzyme binding site during MD simulations.

Besides by hydrogen bonding, aprotinin molecule is stabilized in the enzyme interdomain cleft by numerous hydrophobic interactions that it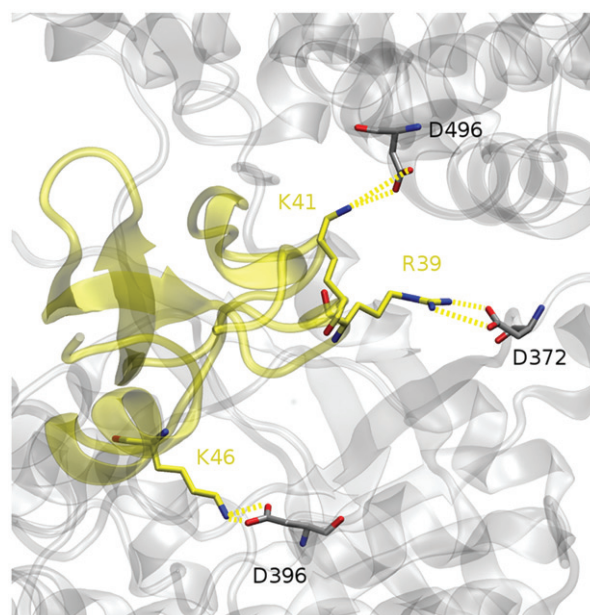 makes with residues that are also part of the hDPP III substrate binding subsites: Tyr10-Ser504, Gly12-His568, Cys14-Ala388, Arg17-Ile386, Ile18-Glu316 and Gly36-Pro387 (written as aprotinin-hDPP III hydrophobic interactions of amino acid residues pair, respectively). Finally, aprotinin backbone rmsd profile also indicates its stability during the productive MD simulations (Figure 5).

Table 3. Intermolecular interactions between selected enzymes and aprotinin amino acid residues.

Aprotinin interaction residues	DPP III (3FVY*)	Trypsin (2PTC)	Chymotrypsin (1CBW)	Dengue virus NS3 protease (3U1J)	Kallikrein (2KAI)	Thrombin (1BTH)	Prostasin (3GYM)	Matriptase (1EAW)
ASP3	HB	–	–	–	–	–	–	–
GLU7	HI	–	–	–	–	–	–	–
PRO8	HB, HI	–	–	–	–	–	–	–
TYR10	HI	–	–	–	–	–	HB	–
THR11		HI	–	–	HI	HI	HI	HI
GLY12	HB, HI		HI	–	HI	–	–	–
PRO13	HI	HB	HB	HB	HB	HB	HB, HI	HB
CYS14	HI	HB	HI	HB	HI	HB	HI	HB
LYS15	HB	HB	HB	HB	HB	HB	HB	HB
ALA16	HI	HI	HI	HI	HI	HI	HI	HB, HI
ARG17	HB, HI	HB	HB, HI	HB	HB, HI	HB	HB, HI	HB
ILE18	HB, HI	–	–	–	HI	HI	–	HI
ILE19	HB, HI	HB	–	HI	–	HI	–	
ARG20	HB	–	–	–	–	HB, HI	–	HB, HI
TYR21	–	–	–	HI	–	–	–	–
LYS26	HB, HI	–	–	–	–	–	–	–
ALA27	–	–	HI	–	–	–	–	–
GLY28	–	–	HI	–	–	–	–	–
THR32		–		HI		HI	–	–
VAL34		–		HI	HI	HB	–	HI
TYR35		–					–	HI
GLY36	HB, HI	–	–	–	HI	–	–	HI
GLY37	HB	HI	HI	HI	HI	HI	HI	–
CYS38	HI	HI		HI		HI		HI
ARG39	HB	HB	HI	–	HB	HB	HB	HB
LYS41	–	–	–	–	–	HI	–	HB
ARG42	HB	–	–	–	–	HI	–	–
ASN43	–	–	–	–	–	HB	–	–
ASN44	–	–	–	–	–	–	–	HB
LYS46	HB	–	–	HB	–	HI	HI	HI
SER47	HB, HI	–	–	–	–	–	–	–
GLU49	–	–	HI	–	–	–	–	–
MET52	–	–	HI	–	–	–	–	–
ARG53	–	–	HI	–	–	–	–	–

Data used for DPP III, trypsin, chymotrypsin, Dengue virus NS3 protease, kallikrein, thrombin, prostasin and matriptase was obtained from the LigPlot + diagrams for PDB codes 3FVY*, 2PTC, 1CBW, 3U1J, 2KAI, 1BTH, 3GYM and 1EAW respectively. *Optimized 3FVY-aprotinin complex obtained after 200 ns of MD simulations. HB and HI are the abbreviations of hydrogen bond and hydrophobic interaction, respectively.

In our study, for the first time, the protein–protein interaction of human DPP III involving the substrate binding region of this enzyme has been demonstrated. Up to date, only hDPP III interaction with the Keap1 protein (Gundić et al., 2016; Hast et al., 2013) has been described. DPP III binds to Kealch domain of Keap1 via the E^{480}TGE^{483} motif situated in the flexible loop on the surface of the "upper" domain and remote from the substrate binding site.

3.5. Electrostatic potential surface and solvent accessible surface area

Strong electrostatic stabilization of the positively charged aprotinin (composed of 4 lysine and 6 arginine residues) with the negatively charged residues, mostly from the hDPP III "lower" domain, is clearly demonstrated by visualization of the electrostatic potential surface calculated by the Adaptive Poisson–Boltzmann Solver (APBS) (Baker, Sept, Joseph, Holst, & McCammon, 2001) module implemented in the program PyMol (Figure 9(A,B)). Electrostatic potential calculated solely for the enzyme molecule extracted from the initial hDPP III-aprotinin complex indicates that the most favorable polypeptide binding mode was predicted to be the one where positively charged aprotinin molecule is situated just above negatively charged protein region next to the five-stranded

β-core of the DPP III "lower" domain (Figure 9(A)), while negatively charged aprotinin residues close to its C and N-terminus are sticking outside of the protein interdomain cleft into the bulk (Figure 9(B,C)). The electrostatic potential surface calculations performed on the enzyme structures obtained during MD simulations of the hDPP III-aprotinin complex revealed that the enzyme binding cleft adjusted to the positively charged aprotinin and became even more negatively charged (structures sampled at 2nd and 200th ns of MD simulation, Figure 9(A)) than in the initial structure. Apparently, the polar protein residues in the binding site reoriented in a way to establish more interactions with aprotinin.

The most important intermolecular electrostatic interactions formed during the MD simulations were Arg39-Asp372, Lys41-Asp496 and Lys46-Asp396 (written as aprotinin-hDPP III amino acid pair, respectively) (Figure 10 and left side of the Supplemental Figure S5 A–C). The bonds existence is confirmed by RDF analyses (right side of the Supplemental Figure S5A–C), where all the maximums are below 3 Å . This finding on important electrostatic interaction of Asp496 with aprotinin is in agreement with the recently reported results of mutational analysis which have shown that replacement of Asp496 with Gly lowered binding potency for aprotinin by 12.7-fold, compared to the wild-type hDPP III (Abramić et al., 2015) indicating the important role of Asp496 in the hDPP III substrate specificity.

In addition, we calculated differences in the solvent accessible surface area (*SASA*) by program Naccess (Naccess version 2.1.1, Faculty of Life Sciences, The University of Manchester, Manchester, UK) (Lee & Richards, 1971) and showed that the initial complex structure used for molecular modeling study has the largest *SASA* (Table 2). The structure obtained after 2 ns of MD simulation has smaller *SASA* than the structure obtained after 200 ns of MD simulation mostly as a result of enzyme side chains being less exposed to water. At the same time, aprotinin molecule seems to be less water exposed in the complex structure obtained after 200 ns of MD simulations, then in the one obtained after 2 ns of MD simulations. This is also mostly due to the aprotinin side chain reorientation, probably in order to establish more favorable electrostatic interactions with protein interdomain cleft.

3.6. Comparison of the aprotinin binding mode in hDPP III with those in the selected serine peptidases

Aprotinin inhibits many serine peptidases, among them and those of viral origin (Mueller, Yon, Ganesh, & Padmanabhan, 2007; Noble, She, Chao, & Shi, 2012). By analyzing the available crystal structures of the aprotinin-serine peptidase complexes we were able to compare the protein–protein intermolecular interactions with those found in the hDPP III-aprotinin complex. Table 3 illustrates that aprotinin residues 13(Pro) to 17(Arg) interact with all examined peptidases through hydrophobic or H-bond interactions, or both. Amino acids Gly37 to Arg39 are also frequently used in aprotinin contacts with peptidases. Our study on hDPP III has shown several additional interactions, not found in other complexes, outside canonical binding epitope. Those are interactions with amino acids near the N-terminus Asp3, Glu7 and Pro8, and with Lys26 and Ser47 (Table 3).

4. Conclusions

In this study, a combined experimental and computational approach was used for investigation of the interaction between the human DPP III, metallopeptidase of the family M49 and aprotinin, polypeptide inhibitor of serine proteinases. Incubation with high concentration of enzyme, followed by MALDI-TOF MS analysis did not show degradation of aprotinin.

Docking of aprotinin into the region of inter-domain cleft of hDPP III and long MD simulations of the enzyme-inhibitor complex revealed that this compact polypeptide interacts with the substrate binding cleft of hDPP III by its canonical binding loop (binding epitope), whereby, the free N-terminus of aprotinin (Arg-Pro-Asp-Phe) is positioned distant from the enzyme active-site, which explains absence of the enzymatic cleavage.

MD simulations suggest that enzyme-inhibitor complex is stabilized by hydrogen bonding, electrostatic and hydrophobic interactions mostly with amino acid residues of the human DPP III S1, S1′, S2, S2′ and S3′substrate binding subsites. To our knowledge, this is the first report on interaction details of aprotinin with a metallopeptidase.

ORCID

Dejan Agić 🅐 http://orcid.org/0000-0002-1154-0710
Hrvoje Brkić 🅐 http://orcid.org/0000-0001-6692-6875
Saša Kazazić 🅐 http://orcid.org/0000-0002-6185-2229
Antonija Tomić 🅐 http://orcid.org/0000-0003-0109-3547
Marija Abramić 🅐 http://orcid.org/0000-0002-2908-3036

References

Abramić, M., Zubanović, M., & Vitale, L. (1988). Dipeptidyl peptidase III from human erythrocytes. *Biological Chemistry Hoppe-Seyler*, *369*(1), 29–38. doi:10.1515/bchm3.1988.369.1.29

Abramić, M., Schleuder, D., Dolovčak, L., Schröder, W., Strupat, K., Šagi, D., … Vitale, L. (2000). Human and rat dipeptidyl peptidase III: Biochemical and mass spectrometric arguments for similarities and differences. *Biological Chemistry*, *381*, 1233–1243. doi:10.1515/BC.2000.151

Abramić, M., Špoljarić, J., & Šimaga, Š. (2004a). Prokaryotic homologs help to define consensus sequences in peptidase family M49. *Periodicum Biologorum*, *106*, 161–168.

Abramić, M., Šimaga, Š., Osmak, M., Čičin-Šain, L., Vukelić, B., Vlahoviček, K., & Dolovčak, L. (2004b). Highly reactive cysteine residues are part of the substrate binding site of mammalian dipeptidyl peptidases III. *The International Journal of Biochemistry and Cell Biology*, *36*(3), 434–446. doi:10.1016/S1357-2725(03)00267-X

Abramić, M., Karačić, Z., Šemanjski, M., Vukelić, B., & Jajčanin-Jozić, N. (2015). Aspartate 496 from the subsite S2 drives specificity of human dipeptidyl peptidase III. *Biological Chemistry*, *396*, 359–366. doi:10.1515/hsz-2014-0247

Agić, D., Brkić, H., Tomić, S., Karačić, Z., Špoljarević, M., Lisjak, M., … Abramić, M. (2017). Validation of flavonoids as potential dipeptidyl peptidase III inhibitors: Experimental and computational approach. *Chemical Biology and Drug Design*, *89*, 619–627. doi:10.1111/cbdd.12887

Ascenzi, P., Bocedi, A., Bolognesi, M., Spallarossa, A., Coletta, M., Cristofaro, R., & Menegatti, E. (2003). The bovine basic pancreatic trypsin inhibitor (Kunitz inhibitor): A milestone protein. *Current Protein and Peptide Science*, *4*(3), 231–251. doi:10.2174/1389203033487180

Baker, N. A., Sept, D., Joseph, S., Holst, M. J., & McCammon, J. A. (2001). Electrostatics of nanosystems: Application to microtubules and the ribosome. *Proceedings of the National Academy of Sciences of the United States of America*, *98*(18), 10037–10041. doi:10.1073/pnas.181342398

Baral, P. K., Jajčanin-Jozić, N., Deller, S., Macheroux, P., Abramić, M., & Gruber, K. (2008). The first structure of dipeptidyl-peptidase III provides insight into the catalytic mechanism and mode of substrate

binding. *Journal of Biological Chemistry*, 283(32), 22316–22324. doi: 10.1074/jbc.M803522200

Baršun, M., Jajčanin, N., Vukelić, B., Špoljarić, J., & Abramić, M. (2007). Human dipeptidyl peptidase III acts as a post-proline-cleaving enzyme on endomorphins. *Biological Chemistry*, 388, 343–348. doi:10.1515/BC.2007.039

Bezerra, G. A., Dobrovetsky, E., Viertlmayr, R., Dong, A., Binter, A., Abramić, M., … Gruber, K. (2012). Entropy-driven binding of opioid peptides induces a large domain motion in human dipeptidyl peptidase III. *Proceedings of the National Academy of Sciences of the United States of America*, 109(17), 6525–6530. doi:10.1073/pnas.1118005109

Broomhead, R. H., Myers, A. E., & Mallett, S. V. (2016). Clinical aspects of coagulation and haemorrhage. *Anaesthesia and Intensive Care Medicine*, 17(2), 86–91. doi:10.1016/j.mpaic.2015.11.002

Capasso, C., Rizzi, M., Menegatti, E., Ascenzi, P., & Bolognesi, M. (1997). Crystal structure of the bovine alpha-chymotrypsin: Kunitz inhibitor complex. An example of multiple protein: Protein recognition sites. *Journal of Molecular Recognition*, 10(1), 26–35. doi:10.1002/(SICI)1099-1352(199701/02)10:1 < 26::AID-JMR351 > 3.0.CO;2-N

Case, D. A., Babin, V., Berryman, J. T., Betz, R. M., Cai, Q., Cerutti, D. S., … Kollman, P. A. (2014). *AMBER 14*. San Francisco: University of California.

Chen, J. M., & Barrett, A. J. (2004). Dipeptidyl-peptidase III. In A. J. Barrett, N. D. Rawlings, & J. F. Woessner (Eds.), *Handbook of proteolytic enzymes (Vol. 1*, pp. 809–812). Amsterdam: Elsevier Academic Press.

Darden, T., York, D., & Pedersen, L. (1993). Particle mesh Ewald: An N. log (N) method for Ewald sums in large systems. *Journal of Chemical Physics*, 98(12), 10089–10092. doi:10.1063/1.464397

Deisenhofer, J., & Steigemann, W. (1975). Crystallographic refinement of the structure of bovine pancreatic trypsin inhibitor at 1.5 Å resolution. *Acta Crystallographica Section B Structural Crystallography and Crystal Chemistry*, 31(1), 238–250. doi:10.1107/S0567740875002415

Engel, M., Hoffmann, T., Manhart, S., Heiser, U., Chambre, S., Huber, R., … Bode, W. (2006). Rigidity and flexibility of dipeptidyl peptidase IV: Crystal structures of and docking experiments with DPIV. *Journal of Molecular Biology*, 355(4), 768–783. doi:10.1016/j.jmb.2005.11.014

Fritz, H., & & Jochum, M. (1989). April). Aprotinin and its targets enzymes *in vitro* and *in vivo*. In D. E. Birnbaum, & H. E. Hoffmeister (Eds.). *Blood saving in open heart surgery – 9th annual meeting of the international society for heart transplantation* (pp. 42–52). Munich, Germany: Schattauer Stuttgart.

Fukasawa, K., Fukasawa, K. M., Kanai, M., Fujii, S., Hirose, J., & Harada, M. (1998). Dipeptidyl peptidase III is a zinc metallo-exopeptidase: Molecular cloning and expression. *Biochemical Journal*, 329(2), 275–282. doi:10.1042/bj3290275

Gabrilovac, J., Abramić, M., Užarević, B., Andreis, A., & Poljak, L. (2003). Dipeptidyl peptidase IV (DPPIV) enzyme activity on immature T-cell line R1.1 is down-regulated by dynorphin-A (1-17) as a non-substrate inhibitor. *Life Sciences*, 73(2), 151–166. doi:10.1016/S0024-3205(03)00257-1

Gundić, M., Tomić, A., Wade, R. C., Matovina, M., Karačić, Z., Kazazić, S., & Tomić, S. (2016). Human DPP III-Keap1 interactions: A combined experimental and computational study. *Croatica Chemica Acta*, 89(2), 217–228. doi:10.5562/cca2916

Hast, B. E., Goldfarb, D., Mulvaney, K. M., Hast, M. A., Siesser, P. F., Yan, F., … Major, M. B. (2013). Proteomic analysis of ubiquitin ligase KEAP1 reveals associated proteins that inhibit NRF2 ubiquitination. *Cancer Research*, 73(7), 2199–2210. doi:10.1158/0008-5472.CAN-12-4400

Helland, R., Otlewski, J., Sundheim, O., Dadlez, M., & Smalås, A. O. (1999). The crystal structures of the complexes between bovine beta-trypsin and ten P1 variants of BPTI. *Journal of Molecular Biology*, 287(5), 923–942. doi:10.1006/jmbi.1999.2654

Huber, R., Kukla, D., Ruhlmann, A., Epp, O., & Formanek, H. (1970). The basic trypsin inhibitor of bovine pancreas I. Structure analysis and conformation of the polypeptide chain. *Die Naturwissenschaften*, 57(8), 389–392. doi:10.1007/BF00599976

Jajčanin-Jozić, N., & Abramić, M. (2013). Hydrolysis of dipeptide derivatives reveals the diversity in the M49 family. *Biological Chemistry*, 394, 767–771. doi:10.1515/hsz-2012-0347

Jorgensen, W. L., Chandrasekhar, J., Madura, J. D., Impey, R. W., & Klein, M. L. (1983). Comparison of simple potential functions for simulating liquid water. *Journal of Chemical Physics*, 79(2), 926–935. doi:10.1063/1.445869

Karačić, Z., Špoljarić, J., Rožman, M., & Abramić, M. (2012). Molecular determinants of human dipeptidyl peptidase sensitivity to thiol modifying reagents. *Biological Chemistry*, 393, 1523–1532. doi:10.1515/hsz-2012-0181

Krowarsch, D., Zakrzewska, M., Smalas, A. O., & Otlewski, J. (2005). Structure-function relationships in serine protease-bovine pancreatic trypsin inhibitor interaction. *Protein and Peptide Letters*, 12(5), 403–407. doi:10.2174/0929866054395275

Kumar, P., Reithofer, V., Reisinger, M., Wallner, S., Pavkov-Keller, T., Macheroux, P., & Gruber, K. (2016). Substrate complexes of human dipeptidyl peptidase III reveal the mechanism of enzyme inhibition. *Scientific Reports*, 6(1), 23787. doi:10.1038/srep23787

Lee, B., & Richards, F. M. (1971). The interpretation of protein structures: Estimation of static accessibility. *Journal of Molecular Biology*, 55(3), 379–400. doi:10.1016/0022-2836(71)90324-X

Mahdy, A. M., & Webster, N. R. (2004). Perioperative systemic haemostatic agents. *British Journal of Anaesthesia*, 93(6), 842–858. doi:10.1093/bja/aeh227

Maier, J. A., Martinez, C., Kasavajhala, K., Wickstrom, L., Hauser, K. E., & Simmerling, C. (2015). ff14SB: Improving the accuracy of protein side chain and backbone parameters from ff99SB. *Journal of Chemical Theory and Computation*, 11(8), 3696–3713. doi:10.1021/acs.jctc.5b00255

Mueller, N. H., Yon, C., Ganesh, V. K., & Padmanabhan, R. (2007). Characterization of the West Nile virus protease substrate specificity and inhibitors. *International Journal of Biochemistry & Cell Biology*, 39(3), 606–614. doi:10.1016/j.biocel.2006.10.025

Nausch, I., Mentlein, R., & Heymann, E. (1990). The degradation of bioactive peptides and proteins by dipeptidyl peptidase IV from human placenta. *Biological Chemistry Hoppe-Seyler*, 371(2), 1113–1118. doi:10.1515/bchm3.1990.371.2.1113

Noble, C. G., Seh, C. C., Chao, A. T., & Shi, P. Y. (2012). Ligand-bound structures of the dengue virus protease reveal the active conformation. *Journal of Virology*, 86(1), 438–446. doi:10.1128/JVI.06225-11

Rastija, V., Agić, D., Tomiš, S., Nikolić, S., Hranjec, M., Karminski-Zamola, G., & Abramić, M. (2015). Synthesis, QSAR, and molecular dynamics simulation of amidino-substituted benzimidazoles as dipeptidyl peptidase III inhibitors. *Acta Chimica Slovenica*, 62, 867–878. doi:10.17344/acsi.2015.1605

Rawlings, N. D., Barrett, A. J., Thomas, P. D., Huang, X., Bateman, A., & Finn, R. D. (2018). The MEROPS database of proteolytic enzymes, their substrates and inhibitors in 2017 and a comparison with peptidases in the PANTHER database. *Nucleic Acids Research*, 46(D1), D624–D632. doi:10.1093/nar/gkx1134

Ryckaert, J. P., Ciccotti, G., & Berendsen, H. J. C. (1977). Numerical integration of the cartesian equations of motion of a system with constraints: Molecular dynamics of n-alkanes. *Journal of Computational Physics*, 23(3), 327–341. doi:10.1016/0021-9991(77)90098-5

Salopek-Sondi, B., Vukelić, B., Špoljarić, J., Šimaga, Š., Vujaklija, D., Makarević, J., … Abramić, M. (2008). Functional tyrosine residue in the active center of human dipeptidyl peptidase III. *Biological Chemistry*, 389, 163–167. doi:10.1515/BC.2008.021

Schechter, I., & Berger, A. (1967). On the size of the active site in proteases. I. Papain. *Biochemical and Biophysical Research Communications*, 27(2), 157–162. doi:10.1016/j.bbrc.2012.08.015

Shimamori, Y., Watanabe, Y., & Fujimoto, Y. (1986). Purification and characterization of dipeptidyl aminopeptidase III from human placenta. *Chemical and Pharmaceutical Bulletin*, 34(8), 3333–3340. doi:10.1248/cpb.34.3333

Špoljarić, J., Tomić, A., Vukelić, B., Salopek-Sondi, B., Agić, D., Tomić, S., & Abramić, M. (2011). Human dipeptidyl peptidase III: The role of Asn406 in ligand binding and hydrolysis. *Croatica Chemica Acta*, 84(2), 259–268. doi:10.5562/cca1808

Tomić, A., Abramić, M., Špoljarić, J., Agić, D., Smith, D. M., & Tomić, S. (2011). Human dipeptidyl peptidase III: Insights into ligand binding

from a combined experimental and computational approach. *Journal of Molecular Recognition, 24*(5), 804–814. doi:10.1002/jmr.1115

Tomić, A., Gonzalez, M., & Tomić, S. (2012). The large scale conformational change of the human DPP III - substrate prefers the "closed" form. *Journal of Chemical Information and Modeling, 52*(6), 1583–1594. doi:10.1021/ci300141k

Tomić, A., & Tomić, S. (2014). Hunting the human DPP III active conformation: Combined thermodynamic and QM/MM calculations. *Dalton Transactions, 43*(41), 15503–15514. doi:10.1039/c4dt02003k

Tomić, A., Kovačević, B., & Tomić, S. (2016). Concerted nitrogen inversion and hydrogen bonding to Glu451 are responsible for protein-controlled suppression of the reverse reaction in human DPP III. *Physical Chemistry Chemical Physics, 18*(39), 27245–27256. doi:10.1039/c6cp04580d

Trott, O., & Olson, A. J. (2009). AutoDock Vina: improving the speed and accuracy of docking with a new scoring function, efficient optimization, and multithreading. *Journal of Computational Chemistry, 31*(2), 455–461. doi:10.1002/jcc.21334

Vio, C. P., Oestreicher, E., Olavarria, V., Velarde, V., Mayfield, R. K., & Jaff, A. A. (1998). Cellular distribution of exogenous aprotinin in the rat kidney. *Biological Chemistry, 379*, 1271–1277. doi:10.1515/bchm.1998.379.10.1271

Webb, B., & Sali, A. (2016). Comparative protein structure modeling using MODELLER. *Current Protocols in Protein Science, 86*, 2–9. doi:10.1002/cpps.20